A Wrench-Sensitive Touch Pad Based on a Parallel Structure

Roger Frigola, Lluís Ros, Francesc Roure, and Federico Thomas

Abstract— **Many different robotic in-parallel structures have been conceived as six-component force sensors. In general, they perform well for most applications but, when accuracy is a must, two main limitations arise. First, in most designs, the legs are connected to the base and the platform through ball-and-socket joints. Although the dry friction in each of these joints can be individually neglected, the integrated effect of twelve such elements becomes noticeable. Second, dynamical measurements might not be very accurate because the natural resonance frequency of the used structures is quite low even for relatively small dimensions. This dynamical response can be obviously modified with a proper mechanical design, but this increases the complexity of the sensor. This paper discusses the design and implementation of a touch pad based on a 6-axis force sensor and shows how the above limitations degrade its behavior. Moreover, it is shown how using a tensegrity structure both problems could be alleviated because ball-and-socket joints can be substituted by point contacts and the resonance frequency of the structure can be controlled by adjusting the static tensions of the tendons.**

Index Terms— **touch pad, force sensor, wrench sensor.**

I. INTRODUCTION

THE Stewart platform is a six degree-of-freedom parallel mechanism proposed by D. Stewart in 1965. Since it is an in-parallel linkage that sustains the payload in a distributive manner, it has high load capacity, and joint errors are not cumulative, as in serial manipulators. Its compact design and interesting properties have prompted different authors to consider it when designing force-torque sensors.

When using a Stewart platform as a force sensor, the platform plays the role of the proof element and the sensing task consists in estimating the forces and torques acting on the platform from those measured at its legs. Legs are attached through ball-and-socket joints to guarantee that forces are only transmitted from the platform to the base along the leg lines.

The development of the first sensor of Stewart platform type based on the octahedral configuration is due to Gaillet and Reboulet [1]. Kerr [2] analyzed a similar structure and enumerated some design criteria for the sensor structure. Other theoretical and experimental investigations were carried out by Romini and Sorli [3], and Sorli and Zhmud [4]. Dasgupta et al. [5] present a design methodology for

Roger Frigola, Lluís Ros, and Federico Thomas are with the Institut de Robòtica i Informàtica Industrial (CSIC-UPC), Llorens Artigas 4-6, 08028 Barcelona, Spain. E-mails: {rfrigola,llros,fthomas}@iri.upc.edu

Francesc Roure is with the Department of Strength of Materials and Structural Engineering (UPC), Avda. Diagonal 647, 08028 Barcelona, Spain. E-mail: francesc.roure@upc.edu

the optimal conditioning of the force transformation matrix. Svinin and Uchiyama [6] have considered the optimality of the condition number of the force transformation matrix. Dwarakanath et al. [7], [8] report an implementation and some experimental results.

This paper presents the design, implementation and performance analysis of a touch pad using a Stewart platform-based force sensor. The paper is organized as follows. Section II introduces the notation and the basic mathematical background. Section III describes the design criteria and the implemented prototype. The experimental results, with particular emphasis on the effects of the different sources of error, are described in Section IV. Section V explains how the obtained accuracy could be improved by transforming the structure into a tensegrity one. The paper is concluded in Section VI summarizing the work.

II. MATHEMATICAL BACKGROUND

Assume we have a platform in static equilibrium, connected to its environment through n legs, articulated with ball-and-socket joints (Fig. 1). Then, every leg applies a force $\mathbf{f}_i$ on the platform, which must be aligned with the leg and, by Poinsot's Central Axis Theorem, any other forces applied on the platform can be reduced to a single force $\mathbf{F}$ and torque $\mathbf{\Gamma}$ acting along the same line l. We will next see how, having sensor readings of the leg forces, we can fully recover $\mathbf{F}$, $\mathbf{\Gamma}$ and the point P where l intersects the platform. In other words, this device can be used as a touch pad with force and torque feedback.

Let f_i and $\mathbf{e}_i$ be the force and the unit vector along leg i, respectively. The resulting wrench of leg forces, $\mathbf{w}_l \in \mathbb{R}^6$, computed with respect to a reference point O on the platform,
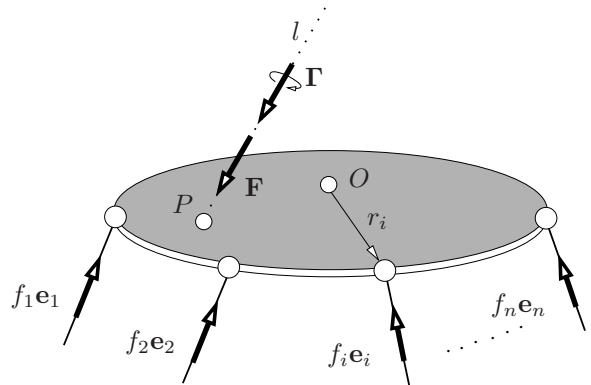

Fig. 1. A platform connected to its environment through n legs.

can be expressed as

$$\mathbf{w}_l = \begin{pmatrix} \sum\limits_{i=1}^{n} f_i \mathbf{e}_i \\ \sum\limits_{i=1}^{n} f_i \mathbf{e}_i \times \mathbf{r}_i \end{pmatrix},$$

where $\mathbf{r}_i$ is the vector going from O to the ith leg attachment point. We can write this in matrix form as $\mathbf{w}_l = \mathbf{J} \cdot \mathbf{f}$, where

$$\mathbf{J} = \begin{pmatrix} \mathbf{e}_1 & \dots & \mathbf{e}_n \\ \mathbf{e}_1 \times \mathbf{r}_1 & \dots & \mathbf{e}_n \times \mathbf{r}_n \end{pmatrix}, \quad \mathbf{f} = \begin{pmatrix} f_1 \\ \vdots \\ f_n \end{pmatrix}.$$

Thus, if we install load cells on the legs to measure the f_i's, $\mathbf{w}_l$ can be easily determined.

Moreover, if we denote by $\mathbf{w}_p = (\mathbf{F}, \mathbf{M})^\top$ the resulting wrench produced by $\mathbf{F}$ and $\mathbf{\Gamma}$ with respect to O, it must be

$$\mathbf{w}_p = \begin{pmatrix} \mathbf{F} \\ \mathbf{F} \times (P - O) + \mathbf{\Gamma} \end{pmatrix}.$$

Since the body is in equilibrium, $\mathbf{w}_p = -\mathbf{w}_l$, and, hence, $\mathbf{F}$ and $\mathbf{M}$ are given by the first and last three components of $-\mathbf{w}_l$, respectively. To isolate $\mathbf{\Gamma}$ from $\mathbf{M} = \mathbf{F} \times (O - P) + \mathbf{\Gamma}$, we use the fact that $\mathbf{F}$ and $\mathbf{\Gamma}$ are aligned, i.e., $\mathbf{\Gamma} = k\mathbf{F}$, for some $k \in \mathbb{R}$. If we choose O in the origin, and let $P = (x, y, z)$, $\mathbf{M}$ becomes:

$$\mathbf{M} = \mathbf{F} \times (x, y, z)^\top + k\mathbf{F}. \tag{1}$$

But if the platform (and hence P) lies on the xy plane, it is $z = 0$, and Eq. (1) together with $z = 0$ define the following system of linear equations

$$\begin{pmatrix} M_1 \\ M_2 \\ M_3 \\ 0 \end{pmatrix} = \begin{pmatrix} 0 & F_3 & -F_2 & F_1 \\ -F_3 & 0 & F_1 & F_2 \\ F_2 & -F_1 & 0 & F_3 \\ 0 & 0 & 1 & 0 \end{pmatrix} \begin{pmatrix} x \\ y \\ z \\ k \end{pmatrix},$$

where the F_i and M_i are the components of $\mathbf{F}$ and $\mathbf{M}$, respectively. If l and $z = 0$ intersect, the system has the unique solution

$$x = \frac{F_1 F_2 M_1 - F_1^2 M_2 - F_3^2 M_2 + F_2 F_3 M_3}{F_3(F_1^2 + F_2^2 + F_3^2)} \tag{2}$$

$$y = \frac{F_2^2 M_1 + F_3^2 M_1 - F_1 F_2 M_2 - F_1 F_3 M_3}{F_3(F_1^2 + F_2^2 + F_3^2)} \tag{3}$$

$$k = \frac{F_1 M_1 + F_2 M_2 + F_3 M_3}{F_1^2 + F_2^2 + F_3^2} \tag{4}$$

which finally gives the coordinates of P explicitly, and allows recovering $\mathbf{\Gamma}$ as $k\mathbf{F}$.

III. THE IMPLEMENTED PROTOTYPE

If $\mathbf{F}$ and $\mathbf{\Gamma}$ can be arbitrarily oriented, then the minimum number of legs needed to compensate them is six. We could use more legs but, to get the simplest possible sensor, we adopted this number in our case. The resulting structure is thus equivalent to a Stewart platform.

Operation constraints required the platform to be circular, with a radius of 0.2 m, and able to support a maximum force of 10 N in any direction. Under these assumptions, the basic

problem is how to arrange the legs so that the load they support is well-distributed among all of them.

To come up with a proper design, we next see how the leg forces vary, as the external wrench $\mathbf{w}_p$ varies within a given ellipsoid of $\mathbb{R}^6$, defined by

$$(\mathbf{w}_p - \mathbf{w}_0)^\top \mathbf{E}_p (\mathbf{w}_p - \mathbf{w}_0) \leq 1. \tag{5}$$

where $\mathbf{w}_0$ is the ellipsoid's center and $\mathbf{E}_p$ is its defining matrix. Assuming the platform's weight is negligible, the ellipsoid will be centered in the origin, and $\mathbf{E}_p$ may easily be derived from the operation constraints above. Substituting $\mathbf{w}_0 = \mathbf{0}$, and $\mathbf{w}_p = -\mathbf{J}\mathbf{f}$ in (5), yields

$$\mathbf{f}^\top \cdot \mathbf{J}^\top \mathbf{E}_p \mathbf{J} \cdot \mathbf{f} \leq 1, \tag{6}$$

and, since $\mathbf{E}_l = \mathbf{J}^\top \mathbf{E}_p \mathbf{J}$ is positive semidefinite, this means the leg forces also take values inside an ellipsoid embedded in $\mathbb{R}^6$. This ellipsoid is centered in the origin, and its semiaxes are defined by the eigenvectors of $\mathbf{E}_l$. Note that, for all leg forces to lie on a same range, it should be

$$\mathbf{J}^\top \mathbf{E}_p \mathbf{J} = \mathbf{I}. \tag{7}$$

In other words, the ellipsoid should ideally be a hypersphere, and the design problem reduces to finding proper vectors $\mathbf{e}_i$ and $\mathbf{r}_i$ satisfying the previous equation.

If, as required, the platform has to support 10 N in any direction, choosing O in its center yields a maximum moment of 2 Nm, meaning that $\mathbf{E}_p = \text{diag}(a, a, a, b, b, b)$, with $a = 1/\sqrt{10}$ and $b = 1/\sqrt{2}$. One can see that, with this $\mathbf{E}_p$, and arranging the legs as depicted in Fig. 2, we obtain a sensor where $\mathbf{E}_l$ nearly defines a hypersphere and is hence close to optimal. Actually, this makes all leg forces lie in the interval ± 7.5 N and, thus, the installed load cells must be able to work within this range. A non-negligible platform weight just changes this interval slightly. It only shifts the ellipsoids for $\mathbf{w}_p$ and $\mathbf{f}$ away from the origin,
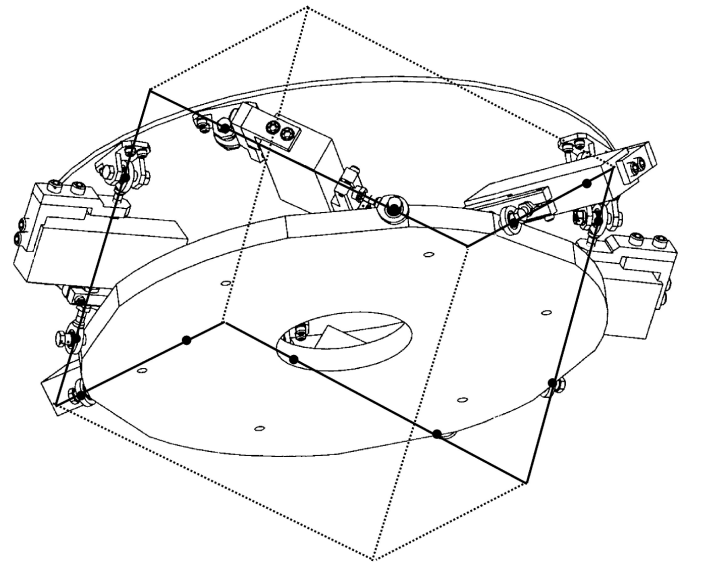

Fig. 2. Conceptual design of the sensor. Legs of length 0.1 m are aligned with the edges of a cube of side 0.3 m.
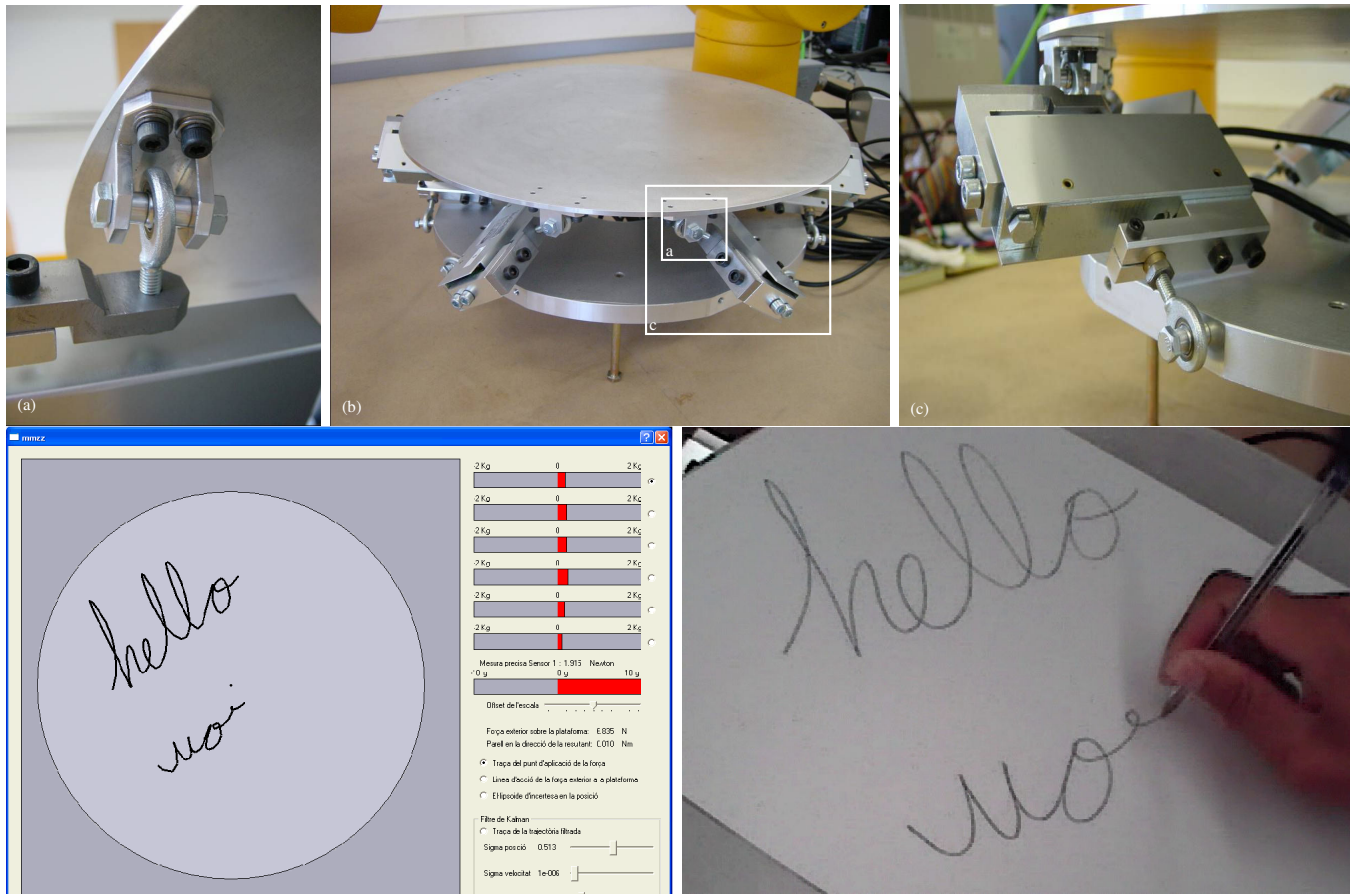
Fig. 3. Top row: Prototype of the sensor (center), details of the used load cells (right), and the ball-and-socket joints (left). Bottom row: a snapshot of the implemented interface (left) when tracking the user's writing during a "hello world" demonstration (right).

keeping their axes' lengths. In our case, the platform has a mass of 2 Kg, which yields an actual interval of leg forces of $[-2.4, 13.6]$ N. A low-cost load cell compatible with this range is Utilcell's 105 model, whose maximum supported force and measurement error are ± 20 N and ± 0.0039 N, respectively.

Fig. 3, top row, shows the constructed prototype, the mounted load cells, and ball-and-socket joints. Bottom row shows a snapshot of the implemented interface (left) when tracking the user's writing during a "hello world" demonstration (right).

IV. PERFORMANCE ANALYSIS

The main problem in the error analysis of the implemented sensor is the study of the sensitivity of P's location to errors in the leg force measurements. This analysis has been carried out using ellipsoidal uncertainty sets [9]. The leg measurement error can be modelled as an ellipsoidal uncertainty set in $\mathbb{R}^6$. That is,

$$(\mathbf{f} - \mathbf{f}_0)^\top \mathbf{E}(\mathbf{f} - \mathbf{f}_0) \leq 1, \qquad (8)$$

where the center of the ellipsoid, $\mathbf{f}_0$, is the actual measurement. Assuming that the error bounds for the six legs are the same, and equal to $\pm\lambda$, the above ellipsoid becomes a sphere of radius λ, with $\mathbf{E} = 1/\sqrt{\lambda}\mathbf{I}$.
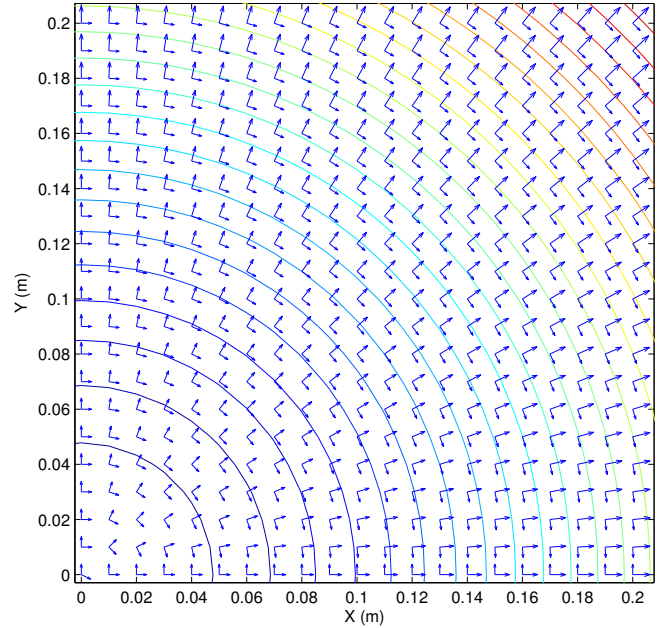

Fig. 4. Semiaxes of the uncertainty ellipsoids in the location of the point contact applying a vertical force of 0.5 N.
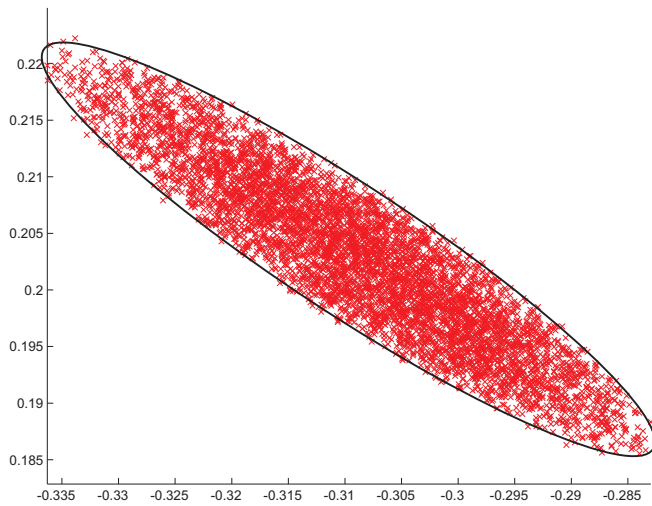
Fig. 5. Contact points obtained assuming that the measurement vector is $\mathbf{f_0} = (0.03, -0.3, 0.03, 0.03, 0.03, 0.3)^\top$ N with an uncertainty of ± 0.0039 N

Fig. 6. A drawing generated using the presented prototype as a touch pad. Dry friction in the ball-and-socket joints induce some artifacts at the end of the strokes (indicated with shadowed circles).

Once we have the uncertainty ellipsoid for the measured forces, we have to propagate it to obtain the uncertainty in the location of the contact point using Eqs. (2) and (3). Since these two equations cannot be expressed in the standard form $\mathbf{A}(x, y)^\top + \mathbf{C}(F_1, F_2, F_3, M_1, M_2, M_3)^\top + \mathbf{d} = \mathbf{0}$, the propagation theorem presented in [9] cannot be applied directly. We have to linearize the relationship between the leg forces and the contact point. After computing the corresponding partial derivatives, we conclude that

$$\mathbf{A} = \begin{pmatrix} -F_3(F_1^2 + F_2^2 + F_3^2) & 0 \\ 0 & -F_3(F_1^2 + F_2^2 + F_3^2) \end{pmatrix}$$

$$\mathbf{C}^\top = \begin{pmatrix} F_2M_1 - 2F_1(M_2 + F_3x) \\ F_1M_1 + F_3(M_3 - 2F_2x) \\ -2F_3M_2 + F_2M_3 - (F_1^2 + F_2^2 + 3F_3^2)x \\ F_1F_2 \\ -F_1^2 - F_3^2 \\ F_2F_3 \end{pmatrix}$$

$$\begin{pmatrix} -F_2M_2 - F_3M_3 - 2F_1F_3y \\ -F_1M_2 + 2F_2(M_1 - F_3y) \\ 2F_3M_1 - F_1M_3 - (F_1^2 + F_2^2 + 3F_3^2)y \\ F_2^2 + F_3^2 \\ -F_1F_2 \\ -F_1F_3 \end{pmatrix}.$$

Fig. 4 shows the semiaxes of the resulting uncertainty ellipsoids in the location of P, when applying a vertical force of 0.5 N with bound errors in the measured leg forces of 0.0039 N. Notice how the semiaxes radially oriented increase as the contact point departs from the center of the platform, while the other semiaxes remain constant.

To evaluate how accurate these results are under the above linearization, we have generated random measurements inside the uncertainty ellipsoid for $\mathbf{f}$ and computed the resulting point on the platform. We have observed that the result is a set of points that can always be perfectly fitted by the ellipsoid obtained using linearization. Actually the linearization errors are small because the errors themselves are small. Fig. 5 shows the set of points resulting from assuming that the measurement vector is $\mathbf{f_0} = (0.03, -0.3, 0.03, 0.03, 0.03, 0.3)^\top$ N with an uncertainty of ± 0.0039 N. Using ellipsoidal propagation and the above linearization, the resulting ellipsoid has semiaxes lengths of 0.0337 m and 0.0062 m, with associated eigenvectors $(-0.836, 0.549)^\top$ and $(-0.549, -0.836)^\top$, respectively.

Measurement errors are not the only source of static errors. When we apply a force on the platform and we release it, we observe that the measurements do not return to their original values. The measurements in the legs are shifted up to 0.25 N in the sense induced by the applied force (see Fig. 6). Applying a short vibration to the platform, the measurements return to their original value. This phenomenon is due to dry friction in the ball-and-socket joints, despite the high quality of the joints employed (INA model GAR 6 UK).

Concerning dynamic errors, Fig. 7-top shows the result of measuring the forces on the six legs during a period of 300 ms, without applying any force on the platform. The platform exhibits a mechanical resonance at about 25 Hz with an amplitude of about 0.05 N. Note how sensors 1, 2, and 4 have opposite phase to that of sensors 3, 5, and 6. Besides this periodic interference, there is background noise with a variance of about 0.006 N. These observations have been confirmed by performing a modal analysis on a finite element model of the sensor. The first four natural frequencies computed on such model are 9.97, 23.57, 27.01, and 32.85 Hz. From a spectral analysis of the signals (see Fig. 7-bottom), it can be seen that only the 23.57 Hz
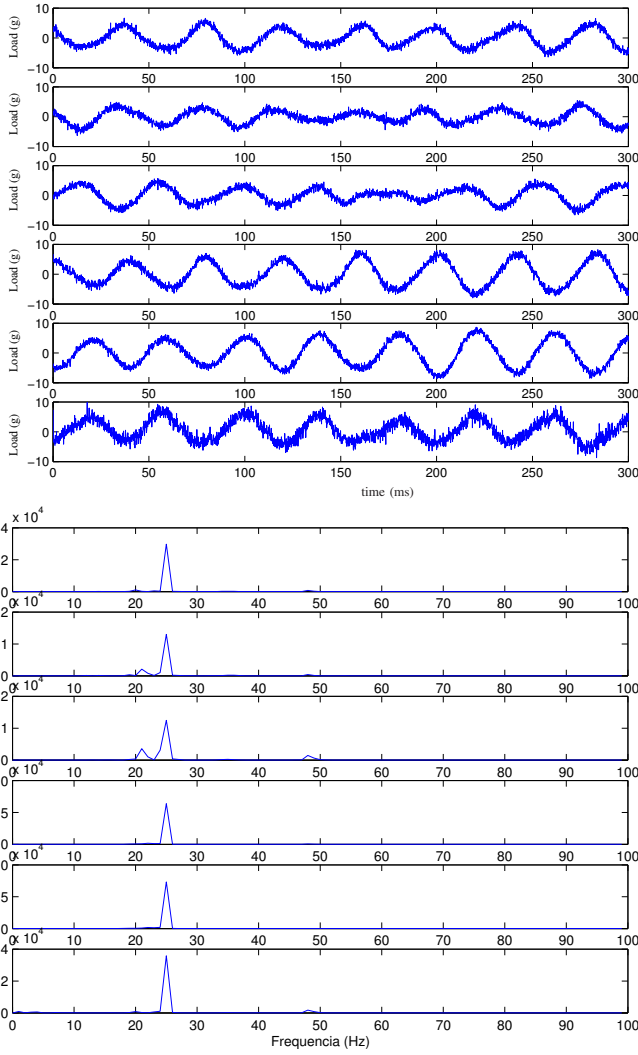
Fig. 7. Top: Signals from the six load-cells with unloaded platform. Bottom: Spectrum of the signals, showing a natural frequency resonance.

frequency is relevant in practice. Using the model, one sees it corresponds to two identical mode shapes in the X and Y directions of the platform.

V. ELIMINATING THE BALL-AND-SOCKET JOINTS

In our prototype, legs are connected to the platform and the base through ball-and-socket joints because they can undergo both tensions and compressions during normal operation (Fig. 9a). If a leg is always in compression, its connections to the rest of the structure can be substituted by point contacts (Fig. 9b). On the contrary, if the leg is always in tension, it can be simply substituted by a tendon (Fig. 9c). So, the problem of eliminating the ball-and-socket joints entails finding alternative structures where all elements during normal operation are always either in tension or compression.

At this point, the architectures proposed in the context of tendon-driven robots are an important source of inspiration. A parallel structure actuated by tendons requires at least

seven wires to allow six degrees of freedom without involving gravity because tendons can only exert traction forces. Then, a clear evolution of our structure in which all legs are substituted by tendons in tension requires an extra tendon pulling the table upwards, as shown in Fig. 8b. Unfortunately, this structure is noticeably unbalanced (six tendons pulling on one side contrasted by only one in the other). In the structure in Fig. 8c, the tendon arrangement guarantees a better distribution of the tensions when an external wrench is applied to the structure. Now, the problem is that the access to the platform is cluttered by tendons. The solution is to substitute the tendons in tension on one side of the table by aligned bars in compression on the other, as shown in Fig. 8d so that the force equilibrium is unaltered. The resulting structure is technically known as a tensegrity structure.

A structure composed of bars and tendons is a tensegrity structure if it has the ability of maintaining an equilibrium shape with all tendons in tension in the absence of external forces. In other words, the integrity of a tensegrity structure is guaranteed by its tendons in tension, hence the denomination, tensegrity, an acronym of tension-integrity coined by R.B. Fuller. The applications of tensegrity structures range from antennas, space telescopes, flight simulators, and deployable structures [10].

Using a tensegrity structure, all ball-and-socket joints can be substituted by point contacts and, as a consequence, dry frictions can be eliminated. Another advantage of this substitution is that dynamic characteristics can be tuned by adjusting the pretension of the structure. The higher the pretension, the higher the natural frequencies. This permits adjusting the fundamental resonance frequency at will.

VI. CONCLUSIONS

We have presented the design and implementation of a force and torque sensor based on a Stewart platform. We have shown how two main sources of error degrade its behavior: the integrated effect of the dry friction in the twelve ball-and-socket joints (which degrade the static measurements), and the mechanical resonance (which degrades the dynamic ones). We have concluded that a structure with a self-stress could provide a good solution to alleviate both problems.

The idea of adopting a self-stressed structure for a force and torque sensor is not new [11]. Nevertheless, the motivation in [11] was not linked to the need of either reducing the dry friction or tuning the structure's natural frequency. The aim was simply to show that structures such as the one in Fig. 8e can effectively be used for force and torque sensing.

Our current work includes implementing a new touch pad based on the above-mentioned tensegrity structures, and extending the finite element model herein developed to tune the tendons' pretensions of the new design.

(a)   (b)   (c)   (d)   (e)
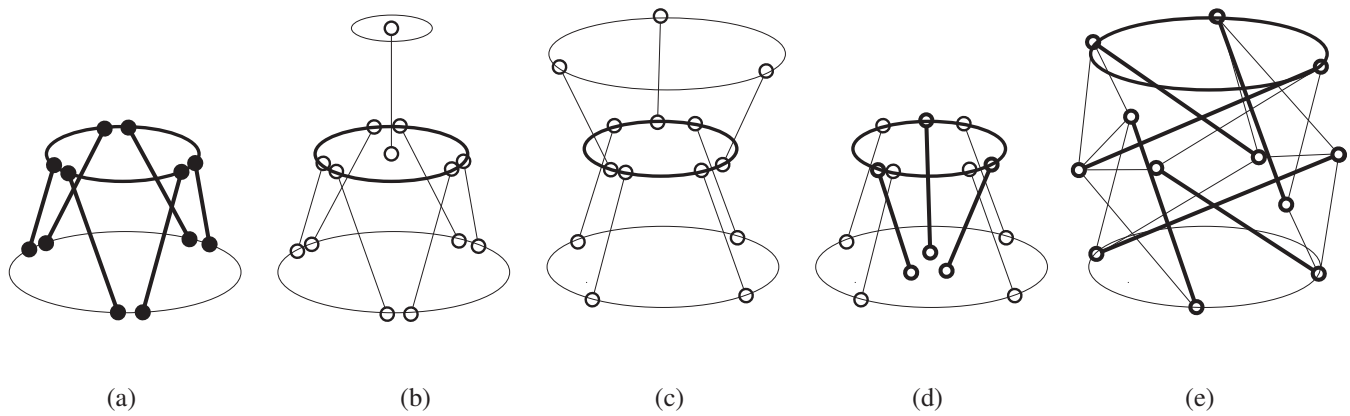
Fig. 8.   Legs in thick lines correspond to rigid bars, while those in thin lines correspond to elastic tendons.
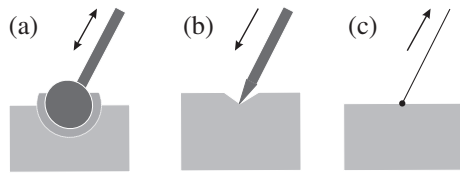

Fig. 9.   A ball-and-socket joint (a) can be substituted by a point contact if it always undergoes either compression forces (b), or expansion forces (c).

REFERENCES

[1] A. Gaillet and C. Reboulet, "An isostatic six-component force and torque sensor," in *Proceedings of the 13th Int. Symposium on Industrial Robotics*, 1983.

[2] D. R. Kerr, "Analysis, properties and design of a Stewart platform transducer," *Trans. ASME, J. Mech. Transm. Automn. Des.*, vol. 111, pp. 25–28, 1989.

[3] A. Romiti and M. D. Sorli, "Force and moment measurement on a robotic assembly hand," *Trans. ASME, J. Mech. Transm. Automn. Des.*, vol. 32, pp. 531–538, 1992.

[4] M. Sorli and S. Pastorelli, "Six-axis reticulated structure force/torque sensor with adaptable performances," *Mechatronics*, vol. 5, no. 6, pp. 585–601, 1995.

[5] B. Dasgupta, S. Reddy, and T. S. Mruthyunjaya, "Synthesis of a force-torque sensor based on the Stewart platform mechanism," in *Proc. National Convention of Industrial Problems in Machines and Mechanisms*, 1994, pp. 14–23.

[6] M. M. Svinin and M. Uchiyama, "Optimal geometric structures of force/torque sensors," *International Journal of Robotics Research*, vol. 14, no. 6, pp. 560–573, 1995.

[7] T. A. Dwarakanath, T. K. Bhaumick, and D. Venkatesh, "Implementation of Stewart platform based force-torque sensor," in *Proceedings of the IEEE/SICE/RSJ International Conference on Multisensor Fusion and Integration for Intelligent Systems*, 1999, pp. 32–37.

[8] T. A. Dwarakanath, B. Dasgupta, and T. S. Mruthyunjaya, "Design and development of a Stewart platform based force-torque sensor," *Mechatronics*, vol. 11, no. 7, pp. 793–809, 2001.

[9] L. Ros, A. Sabater, and F. Thomas, "An ellipsoidal calculus based on propagation and fusion," *IEEE Transactions on Systems, Man, and Cybernetics - Part B: Cybernetics*, vol. 32, no. 4, pp. 430–442, 2004.

[10] R. Motro, *Tensegrity. Structural Systems for the Future*. Kogan Page Science, London and Sterling, VA, 2003.

[11] C. Sultan and R. Skelton, "A force and torque tensegrity sensor," *Sensors and Actuators A*, vol. 112, pp. 220–231, 2004.